Nanoscale

PAPER

View Article Online
View Journal | View Issue

Cite this: *Nanoscale*, 2025, **17**, 24682

The cellular response of the bronchial epithelium shapes the protein corona of inhaled nanoparticles

Daniel Sanchez-Guzman, †[a] Chloé Chivé,[a] Olivier Taché,[b] Marco P. Monopoli,[c] Armelle Baeza-Squiban[a] and Stéphanie Devineau *[a,b]

Protein adsorption to nanoparticles is a key molecular event that influences their fate, biodistribution and toxicity. In the lung, a mucus layer protects the bronchial epithelium from inhaled pollutants. However, the effect of cell exposure to nanoparticles on the formation of the protein corona in the bronchial mucus is not well understood. This study aimed to uncover how the bronchial epithelial cell response shapes the biomolecular corona on inhaled nanoparticles and whether cell adaptation remodels the nano/bio interface. We reproduced a realistic scenario of lung exposure to silver nanoparticles (AgNPs) *in vitro* using a 3D human bronchial epithelium model. AgNPs were incubated in the isolated bronchial mucus or directly exposed to Calu-3 cells at the air–liquid interface. The stability of AgNPs in the mucus was characterized by small-angle X-ray scattering, dynamic light scattering, and transmission electron microscopy. The protein corona formed during the exposure of the bronchial epithelium to nanoparticles was analyzed using quantitative mass spectrometry and Reactome pathway analysis as a function of NP concentration and exposure time. Proteomic analysis revealed major differences in the biomolecular corona formed *in situ* compared to the corona formed in isolated bronchial mucus. Unique proteins expressed in the apical secretome of Calu-3 cells exposed to AgNPs were identified in the protein corona formed *in situ*. The stress response of the epithelial cells led to a complete reshuffling of the protein corona after initial deposition of AgNPs on mucus. Our results demonstrate that the cellular response of the bronchial epithelium plays a critical role in shaping the protein corona of inhaled particles. The remodeling of the nano/bio interface by cellular secretory mechanisms during exposure calls for a renewed focus on the role of cells and NP-cell interactions in biomolecular corona studies using advances 3D models.

Received 17th June 2025,
Accepted 7th October 2025

DOI: 10.1039/d5nr02590g

rsc.li/nanoscale

Introduction

The inhalation of natural or engineered airborne nanoparticles (NPs, defined as particles with a diameter < 100 nm) is a critical route of exposure, especially in occupational settings. The potential adverse effects of inhaled NPs depend on their ability to induce cellular effects, such as oxidative stress, pro-inflammatory effects or the activation of the immune system in the lungs, and on their ability to cross the epithelial barriers at the bronchial and alveolar level, which may result in systemic toxicity.

In the bronchi, the epithelium is protected by a mucus layer of 25–30 μm that acts as the first line of defense against pathogens and particles, while the alveoli are covered by a thin layer of pulmonary surfactant of 0.1 μm that preserves the alveolar structure during breathing.[1] When NPs are deposited in the respiratory tract, proteins present in biological fluids adsorb onto the NP surface to form a protein corona (also called a biomolecular corona or biocorona).[2] This biological layer mediates the interaction of NPs with cells and is often designated as the new 'biological identity' of NPs. It plays a major role in the toxicity and biodistribution of NPs.[3,4] However, little is known about the formation of the protein corona following inhalation of NPs.

The protein corona differs from the bulk composition of the surrounding biological medium. Some proteins are enriched, while others are depleted depending on their affinity for the surface, a pattern specific to the composition of both the particles and the biological medium. In addition, the protein corona undergoes dynamic evolution over time through continuous protein exchange and conformational changes in adsorbed proteins.[5] As the protein corona forms in biological systems that can comprise thousands of different

[a]*Université Paris Cité, CNRS, Unité de Biologie Fonctionnelle et Adaptative, 75013 Paris, France. E-mail: stephanie.devineau@u-paris.fr*
[b]*Université Paris-Saclay, CEA, CNRS, NIMBE, 91191 Gif Sur Yvette, France*
[c]*Department of Chemistry, Royal College of Surgeons in Ireland (RCSI), 123 St Stephen Green, Dublin 2, Ireland*
†Current address: Institute of Cancer Research, Centre for Cancer Drug Discovery, London, UK.

proteins, its composition has proved difficult to control despite efforts to prevent protein adsorption on NPs for drug delivery applications.[6] The adsorption of other biomolecules, such as lipids or polysaccharides, presents additional complexity and analytical challenges to this picture.[7,8]

Nanotoxicology studies have shown that protein corona can increase and decrease the toxicity of NPs.[9–12] To understand these effects, great efforts have been made over the past decade to characterize the biomolecular corona, define the chemical and biochemical determinants of protein-NP interactions and identify pathways that could link the protein corona to different toxicological outcomes.[13–17] Both specific and nonspecific mechanisms can be involved: NP internalization and translocation can be enhanced by direct binding of proteins to extracellular receptors,[18] NP phagocytosis by macrophages can be inhibited in the absence of opsonins in the protein corona,[19] and protein fibrillation can be triggered by structural alterations induced by adsorption on NP surface.[20] Pisani *et al.* showed that the protein corona formed in foetal bovine serum increased the toxicity of silica NPs for HepG2 cells compared to the same particles with a protein corona formed in human serum.[21] The identification of the protein corona is thus an important parameter to determine the biological effects of nanomaterials in toxicological studies.

The protein corona has been initially analyzed after incubating NPs in a biological fluid of known composition, such as plasma, serum, digestive enzymes, or cell extracts. Molecular dynamics simulations have also been developed to predict protein-NP interactions *in silico*.[22,23] Although these approaches are valuable for analyzing the formation of the protein corona on various NPs, they do not integrate the cellular response in this process and lack realistic conditions for a specific exposure scenario.[24] Cells exposed to NPs may secrete biomolecules that change the composition of the extracellular environment, such as cytokines that modulate the inflammatory cell response. Moreover, NPs elicit a variety of intracellular responses depending on their physical and chemical properties.[25] The uptake and intracellular accumulation of NPs in endosomes and lysosomes, which has been shown to induce lysosomal dysfunction,[26,27] also leads to the rearrangement of the protein corona through protein desorption and adsorption inside the organelles.[28] Furthermore, the intracellular exchange of extracellular proteins, such as blood plasma proteins, from the corona to the cell cytoplasm could alter proteostasis and interfere with cell metabolism.[29] To take into account such effects, analytical methods were developed to extract or probe the intracellular protein corona, such as fluorescent or photocatalytic protein proximity labelling,[30,31] isotope labelling and NMR,[32] fluorescence correlation spectroscopy,[33] surface-enhanced Raman scattering,[34] flow cytometry,[35] organelle separation[29] or PFA cross-linking.[36] The protein corona that forms when cells are exposed to NPs is often referred to as an *in situ* protein corona in the literature, as opposed to the corona that forms in biological fluids in a tube, even though an isolation step is often necessary to analyse the adsorbed proteins.[37,38] When cells are absent, the protein corona is formed in a closed system whose composition is initially fixed and homogeneous. While protein adsorption can take place in cell-free conditions, it lacks the cellular input that is associated with cell exposure to NPs. These effects include the secretion of biomolecules into the extracellular microenvironment and the uptake and distribution of NPs within different cellular compartments, where macromolecular crowding may further destabilize NPs and the biomolecular corona.[39]

The analysis of the biomolecular corona *in vitro*, *in vivo*, and *ex vivo*, combined with technical advances in identifying and quantifying adsorbed biomolecules has been an active area of research.[12,15–17,40,41] Techniques for separating NPs from free proteins have also evolved, from centrifugation and magnetic separation,[42] to the development of size exclusion chromatography, flow-field-flow fractionation and microfluidic devices for recovering NPs with their hard and/or soft protein corona.[38] Using an *in vitro* model, Albanese *et al.* showed that the exposure of HeLa cells to gold NPs led to the secretion of proteins that in turn modify the stability and aggregation state of NPs in the conditioned medium.[43] By comparison, few studies analysed the composition of the protein corona *in vivo*, in part due to the difficulty to recover NPs in the organism after exposure.[40] Li *et al.* showed that graphene oxide sheets induce higher lung injury in mice when they were covered by a protein corona with the lowest content in serum proteins.[12] Hadjidemetriou *et al.* reported that the protein corona formed *in vivo* after intravenous infusion of PEGylated liposomes in mice and in humans differs from the one formed *in vitro* in mouse or human plasma respectively.[44] Local concentration effects, such as the release of platelet proteins in injured blood vessels, have been associated with the formation of a transient protein corona with higher binding properties for endothelial cells.[45] Several factors may modify the protein corona *in vivo*, such as the effect of blood flow on protein adsorption,[41,46] the interaction of NPs with circulating blood cells,[47] or the immune response to the injected liposomes,[48] but the origin of the protein corona dynamics cannot be easily defined *in vivo*.

Finally, few studies analysed the formation of the protein corona in the respiratory tract lining fluids such as human respiratory tract lining fluid (RTLF)[49] or non-human bronchoalveolar lavage fluids (BALF),[50] which are relevant to exposure by inhalation of NPs.[23] Moreover, inhaled pollutants can modify the production of mucus by the bronchial epithelial cells both in quantity and in composition.[51] Thus, the epithelial response to exposure to airborne pollutants is likely to modify the composition of the protein corona, an effect that cannot be reproduced in cell-free conditions.

The objective of this study is to reproduce a realistic scenario of exposure to inhaled NPs *in vitro* and to investigate whether the response of the bronchial epithelial cells changes the protein corona. We used a 3D model of a mucus-producing bronchial epithelium obtained by differentiation of Calu-3 cells at the air–liquid interface (ALI). This approach is in line with the 3R strategy for animal use alternatives in toxicological studies. The bronchial cells form a tight and functional epi-

thelium where the apical side is protected by a native mucus layer. The secreted mucus contains more than 400 extracellular proteins involved in the lung epithelial and immune function. We showed in a previous study that the composition of the mucus was highly similar between Calu-3 cell lines and primary NHBE (Normal Human Bronchial Epithelial) cells, making it a good model for the study of the protein corona on inhaled NPs compared to other sources of mucus proteins such as lyophilized mucins.[52]

Silver nanoparticles (AgNPs) present a risk to human health due to their wide use for commercial and biomedical applications, with the development of novel, silver-based nanomedicines.[53–55]. Inhalation of AgNPs may occur following the use of face masks treated with antibacterial AgNPs or hygiene sprays, and in occupational settings during the synthesis of AgNPs and the preparation of silver-coated products. Despite their widespread use, the application of AgNPs as therapeutic agents is still being debated, due to concerns about their toxicity and potential accumulation in organs.[56,57] The lung toxicity of AgNPs was reported both *in vitro* and *in vivo*.[58–62] Depending on the toxicity endpoint considered, NOAECs (No Observed Adverse Effect Concentration) ranging from 110 to 750 μg m^{-3} were reported following the inhalation of AgNPs of different sizes.[63] An exposure limit of 0.19 μg m^{-3} has been suggested by Weldon *et al.* based on a sub-chronic inhalation study in rats.[64] These limits are likely to depend on the size, functionalization, and dissolution kinetics of AgNPs, a parameter that is biologically mediated by the adsorbed proteins at the surface of AgNPs.[65] Here, we propose to investigate the formation and the evolution of the protein corona, and the cellular response to inhaled AgNPs in a human bronchial epithelium model as a determinant of AgNP toxicity in the respiratory tract.

The bronchial epithelium was exposed to AgNPs at the ALI for 1 h and 24 h at a concentration of 10 to 50 μg cm^{-2} corresponding to a low and high dose of AgNPs.[59] In parallel, the mucus was collected from unexposed cells and incubated with AgNPs in cell-free conditions. The physical and chemical stability of AgNPs was fully characterized in the bronchial mucus by small angle X-ray scattering (SAXS), dynamic light scattering (DLS), and transmission electron microscopy (TEM). The epithelial cell response and the composition of the 'cellular' and 'acellular' protein corona were monitored by biological assays and quantitative proteomics after 1 h and 24 h exposure. Unique proteins expressed in the secretome of Calu-3 cells treated with AgNPs were identified in the protein corona formed *in situ*. Our results demonstrate that the cellular response of the bronchial epithelium plays a crucial role in shaping the protein corona of inhaled NPs.

Results

Our experimental strategy is presented in Fig. 1A. A functional 3D model of the human bronchial epithelium was developed by cultivating Calu-3 cells on a porous insert, followed by differentiation of the epithelial cells at the ALI. After 10 days, the bronchial epithelium generates a mature, protein-rich mucus layer, designated the apical secretome.[52] The protein corona that forms on AgNPs in the mucus secreted by Calu-3 cells was analyzed in acellular and cellular conditions, that is, with and without exposure of the bronchial epithelium to AgNPs.

In acellular conditions, AgNPs were incubated for 1 h in the bronchial mucus collected from unexposed cells. In cellular conditions, the bronchial epithelium was exposed to AgNPs at the ALI for 1 h and 24 h. The apical secretome was then collected to analyse the protein corona of AgNPs that remained in the mucus layer. The cellular protein corona refers here to the corona formed in the apical secretome of Calu-3 cells treated with AgNPs. It does not correspond to the intracellular corona of AgNPs inside cells, unless released in the cell microenvironment. An equivalent particle concentration of 10 and 50 μg cm^{-2} was used in both conditions. Control cells were treated with HBSS buffer.

Stability of AgNPs in the bronchial mucus

First, the size and stability of AgNPs were analyzed in H_2O stock suspension, in $HBSS^{Ca^{2+}/Mg^{2+}}$ buffer used for cell exposure, and in the apical secretome of Calu-3 cells (Fig. 1). TEM, DLS, and SAXS were used as complementary techniques to measure the size distribution of AgNPs in different media: the diameter of dried particles was measured by TEM, the hydrodynamic diameter by DLS, and the radius of gyration in viscous mucus by SAXS. AgNPs were analyzed by TEM in H_2O stock suspension after drying, after 1 h incubation of AgNPs in the bronchial mucus, and after 1 h exposure of Calu-3 cells to AgNPs at the ALI (Fig. 1B–D). The mean diameter measured in H_2O was 25 ± 5 nm. The TEM images of AgNPs incubated in the bronchial mucus without cells show well-defined spherical particles without any agglomeration or aggregation (Fig. 1C). To image AgNPs in cellular conditions, we fixed the bronchial epithelium after 1 h exposure to AgNPs using an adapted protocol to preserve the mucus layer.[66,67] The TEM images of the thin sections revealed AgNPs trapped in the mucus network above the microvilli that form the epithelial brush border (Fig. 1D).

To complete the size analysis, the hydrodynamic diameter of AgNPs was measured by DLS in $HBSS^{Ca^{2+}/Mg^{2+}}$, which is the buffer used to collect the bronchial mucus and for cell exposure to AgNPs. Two populations were identified by DLS with hydrodynamic diameters of 35 ± 10 nm and 4.5 ± 1.0 nm respectively (Fig. 1E), reflecting the size distribution of NM-300 K AgNPs reported in JRC report.[68]

The stability of AgNPs in the bronchial mucus was analysed by SAXS, which can be performed on small volumes (50 μL) of viscous suspensions such as mucus. SAXS provides a better resolution than DLS for the size metrology of NPs in suspensions and allows measuring the particle concentration. The intensity of scattered light $I(q)$ measured by SAXS for AgNPs incubated for 1 h, 24 h, and 48 h in the bronchial mucus and for control AgNPs in H_2O is shown in Fig. 1F. No significant

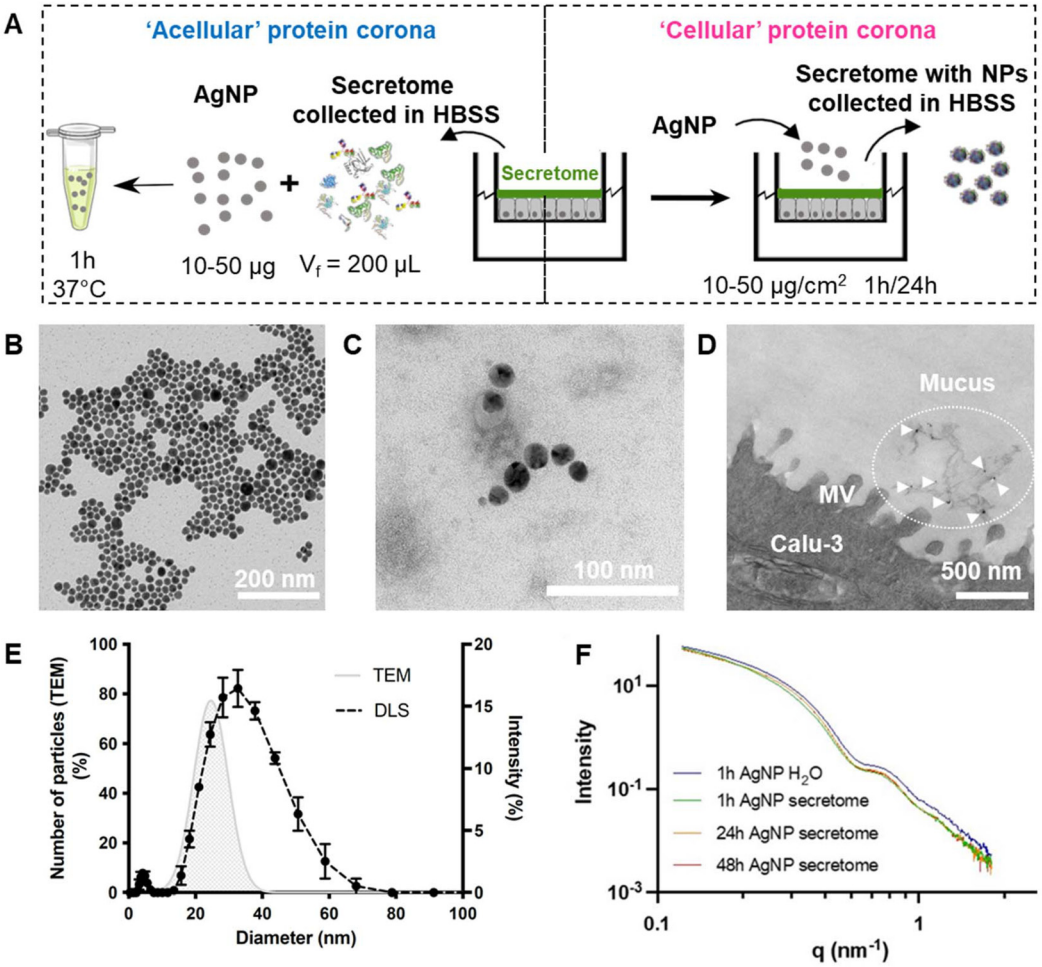

Fig. 1 Characterization of AgNPs in H_2O, in HBSS and in the bronchial mucus. (A) Experimental design for the formation of the protein corona by exposure of Calu-3 cells to AgNPs (right) or by incubation of AgNPs in the bronchial mucus without cells (left). (B–D) TEM image of (B) dried AgNPs, (C) AgNPs after 1 h incubation in the bronchial mucus in acellular condition, (D) thin section of Calu-3 cells after 1 h exposure to AgNPs at the ALI. White arrows indicate AgNPs trapped in the mucus. m: microvilli. (E) Size distribution of AgNPs measured by TEM on AgNP suspension in H_2O after drying, and by DLS on AgNP suspension in HBSS. TEM data are represented by a Gaussian distribution of particle sizes measured for 2500 particles. (F) SAXS profile of AgNPs after incubation in H_2O and in the bronchial mucus for 1, 24, and 48 h. Data are presented as $I(q)/q^3$.

difference was observed between water and the apical secretome with a mean diameter of 14.7 ± 2.6 nm in H_2O and 15.1 ± 2.7 nm in the apical secretome after 1 h incubation. AgNPs were stable over time with a mean diameter of 15.5 ± 2.3 nm after 24 and 48 h incubation in the apical secretome. These results are in good agreement with the interlaboratory comparison of AgNPs by TEM provided by the JRC.[68] It confirms that AgNPs do not agglomerate or aggregate in the bronchial mucus.

If dissolution occurs, the particle diameter and concentration would decrease as a result of the faster dissolution kinetics of the smallest particles. No significant decrease in particle concentration was observed over time in the secretome with an average concentration of $2.7 \pm 0.1 \times 10^{14}$ particles per mL after 1 h and 24 h incubation and $2.6 \pm 0.1 \times 10^{14}$ particles per mL after 48 h incubation. The absence of dissolution of AgNPs in the apical secretome of Calu-3 cells was confirmed after incubation of AgNPs for 18 days at 37 °C in a previous study.[59] As AgNP dissolution was reported in Lung Simulant Fluid that does not contain proteins,[69] it suggests that the formation of a protein corona in the bronchial mucus may stabilize and protect AgNPs from dissolution.

Formation of the acellular protein corona in the bronchial mucus

To form a corona in acellular conditions, 10 and 50 µg AgNPs were incubated in the bronchial mucus without cells. AgNP concentration in the mucus corresponds to cell exposure to 10 and 50 µg cm^{-2} AgNPs after collecting the apical secretome in 200 µL of HBSS. The bronchial mucus was pooled to keep the same protein concentration and composition in all the conditions.

We adapted the protocol to isolate the protein corona of AgNPs in the bronchial mucus to avoid the precipitation of

free proteins during centrifugation (Fig. S1A).[70] The apical secretome is a viscous medium composed of high molecular weight proteins that tend to sediment if a standard protocol for NP separation by centrifugation is applied. We observed that a freeze/thaw cycle at −80 °C followed by a low-speed centrifugation reduced the precipitation of free proteins, possibly by destabilizing the mucus network. No proteins were detected in the control samples by SDS-PAGE using fluorescence detection (Fig. S1B). To avoid false positives in mass spectrometry analysis, the same isolation protocol was applied to the apical secretome of control cells. The proteins identified by LC-MS/MS in the pellet of the control samples were excluded from the protein list of the corona.

The acellular corona was analysed by quantitative mass spectrometry to identify the adsorbed proteins and determine their relative abundance (Fig. 2). 73 and 90 proteins were identified in the protein corona of 10 and 50 μg AgNPs respectively (Fig. 2A). 65 common proteins were identified independently of AgNP concentration. In addition, 8 proteins were specific to the corona formed at low NP concentration, while 25 were specific to high NP concentration, which indicates that the diversity of the protein corona increases with the available surface area. With a 5-fold increase of the surface area from 10 to 50 μg AgNPs, it suggests that competition for adsorption decreased and allowed more proteins to bind to the surface.[71] A total of 1685 proteins have been identified in the bronchial mucus of Calu-3 cells.[52] The small number of proteins identified here can be explained in part by the removal of proteins identified in the control samples labelled as false positive, as we cannot exclude that they can also be part of the corona.

A gene ontology analysis was applied to identify the intracellular and extracellular proteins in the acellular corona (Fig. 2B). It is composed of 63% intracellular and 37% extracellular proteins. A similar ratio was observed for the acellular corona formed at low and high AgNP concentration. The prevalence of intracellular proteins in the acellular corona is not surprising as they represent 75% of the proteins identified in the mature secretome of Calu-3 cells.[52] We chose not to exclude the intracellular proteins from the analysis as they can be part of the protein corona both *in vitro* and *in vivo* following cell death and the renewal of the epithelial barrier. In proteomics studies of extracellular matrices, a filter is often applied on proteomics data to select the extracellular proteins only, so that the fraction of intracellular proteins is often shielded. Our results show that they are present in the mucus secreted by the bronchial epithelium and that they contribute to the formation of the corona *in vitro*.

Among the extracellular proteins identified, the acellular corona is enriched in interleukin-18 (IL-18) pro-inflammatory cytokine and in midkine (MDK) growth factor that plays a role in cell growth and in the epithelial–mesenchymal transition of cancerous cells. A majority of the extracellular proteins (up to 90%) can be classified as proteins associated with extracellular vesicles (EV), which reflects their role in airway secretions as shown by Gupta *et al.*[72] Note that the classification of exosomal proteins may differ from one database to another.[73]

We observed that the relative abundance of proteins in the acellular corona depends on AgNP concentration (Fig. 2C and D). The list of the 10 most abundant proteins in each condition is provided in Table S2. The acellular corona is enriched in proteasome proteins (PSMB3, PSMB4, and PSMB7) and RNA-binding protein (EWSR1, LUC7L2). As we identified several subunits of the proteasome complex, it is likely that the complex is directly or indirectly bound to AgNPs through protein–surface or protein–protein interactions. At high NP concentration, the corona is enriched in RNA-binding (YBX1) and DNA-binding (HMGB3) proteins, which suggests a high affinity of RNA- and DNA-binding proteins for AgNPs.

To gain more insights into the role of the acellular corona, the biological function of the adsorbed proteins was examined using a Reactome pathway analysis, which considers protein interactions within a functional network. Both the protein relative abundance and the number of proteins involved in each pathway are taken into account. We considered that a biological pathway was identified when at least 10 different proteins were present in the corona and that it was significantly enriched if $p < 0.05$. The results are presented in Fig. 2E. The biological pathway for the metabolism of amino acids was significantly enriched in the acellular corona and common to 10 and 50 μg AgNPs. At 50 μg AgNP, two additional biological pathways were significantly enriched in the acellular corona for the metabolism of RNA and the response to infectious disease, reflecting the richer composition of the corona at high NP concentration.

The detection of protein networks in the protein corona suggests two possible mechanisms. In the first assumption, the protein network is reduced to proteins belonging to the same complex, which may bind to AgNPs through a combination of protein–surface and protein–protein interactions, as shown for chaperonins. However, if proteins do not directly interact within a protein network, another possible mechanism is that proteins involved in the same function may share structural or chemical features that favour their adsorption to AgNPs. This mechanism was demonstrated for the family of RNA-binding proteins, which have a strong affinity for silica NPs in the absence of DNA.[74] The enrichment of the biological pathway associated with the metabolism of RNA together with the high relative abundance of RNA- and DNA-binding proteins in the acellular corona suggests that a similar mechanism may take place for AgNPs.

Formation of the protein corona during cell exposure to AgNPs

The cytotoxicity of AgNPs was monitored during exposure of Calu-3 cells at the ALI to 10 and 50 μg cm^{-2} AgNPs for 1 h, 24 h, and 48 h. After differentiation at the air–liquid interface, the bronchial epithelial cells stop proliferating and form a stable epithelial barrier. The epithelial cells were exposed 10 days after ALI induction, when a mature apical secretome is produced.[52] No significant change of the cell morphology and ultrastructure was observed following 5 repeated exposures to AgNPs at 10 μg cm^{-2} in a previous study.[59] The measurement of the Trans Epithelial Electric Resistance (TEER) and Lucifer Yellow (LY) permeability show that the epithelial barrier integ-

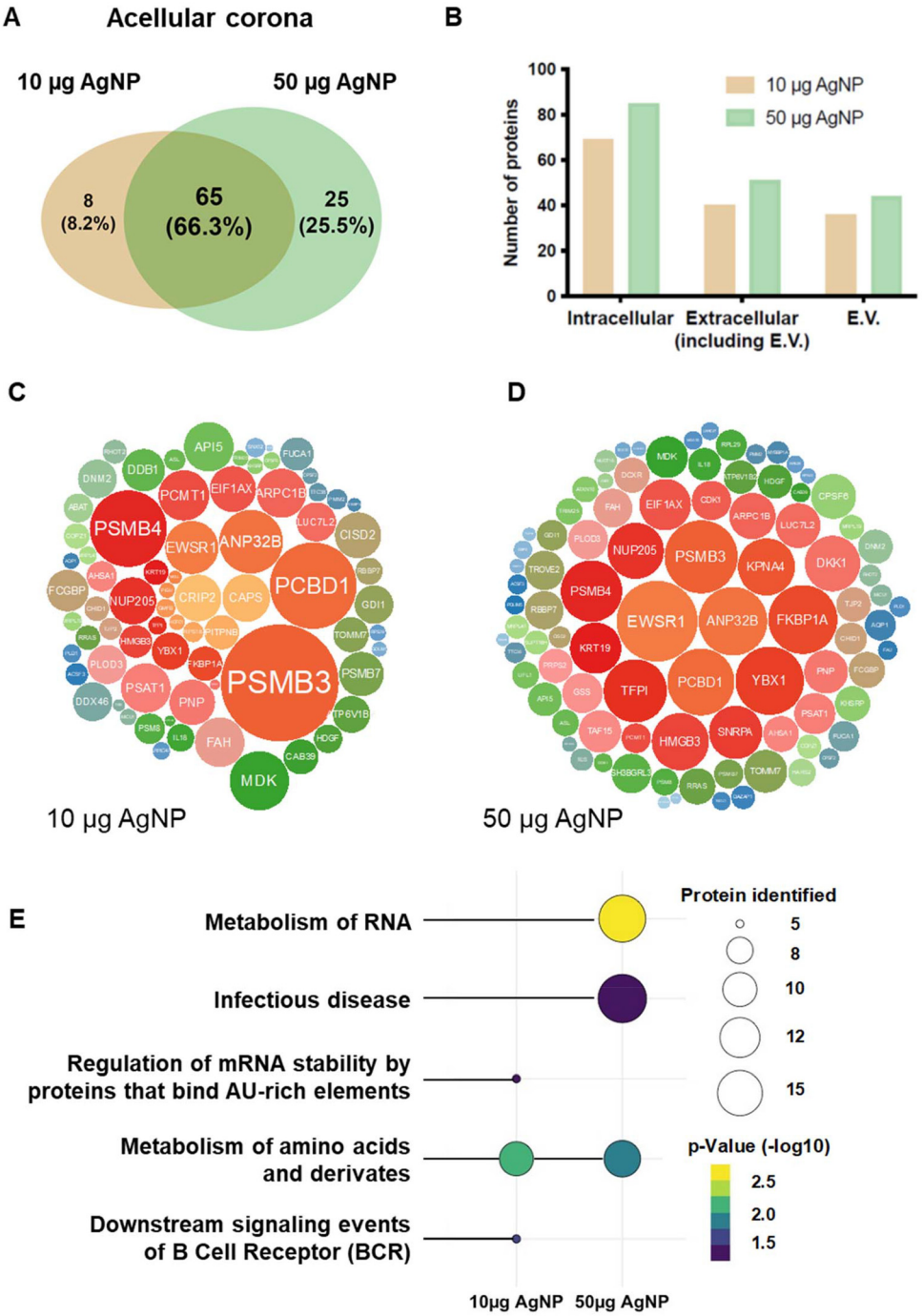

Fig. 2 Proteomic analysis of the acellular protein corona of AgNPs formed in cell-free condition in the bronchial mucus. (A) Venn diagram of protein corona composition for 10 and 50 µg AgNP. (B) Total number of intracellular proteins, extracellular proteins (including EV proteins), and proteins associated to extracellular vesicles (EV). (C and D) Relative protein abundance in the protein corona for 10 and 50 µg AgNP. (E) Reactome pathway analysis of the protein corona. Circle size reflects the number of proteins associated with each pathway. A minimum of 10 different proteins must be identified to validate a functional pathway. Only pathways significantly enriched in the corona are shown ($p < 0.05$).

rity was preserved in all the conditions (Fig. S2). The metabolic activity did not significantly change compared to control cells exposed to HBSS buffer only, except for treatment at 10 µg cm^{-2} AgNPs for 48 h where a small decrease was recorded. Based on these results, we chose to expose Calu-3 cells at the ALI to non-cytotoxic concentrations of 10 and 50 µg cm^{-2} AgNPs for 1 h and 24 h for the analysis of the protein corona *in situ*.

The proteomic analysis revealed a more diverse and richer protein corona composed of 367 and 377 different proteins

after exposure of Calu-3 cells to 10 and 50 μg cm^{-2} AgNPs for 24 h, compared to 100 and 104 proteins after 1 h (Fig. 3A and B). Only 10% of the adsorbed proteins were common to the cellular corona formed after 1 h and 24 h exposure, showing that a major reshuffling of the protein corona of AgNPs took place during cell exposure. These changes were associated both with the removal of proteins adsorbed at 1 h (57 and 53 proteins at 10 and 50 μg cm^{-2}) and with the adsorption of new proteins after 24 h exposure (324 and 327 proteins at 10 and 50 μg cm^{-2}). By comparison, 76% and 85% of the proteins

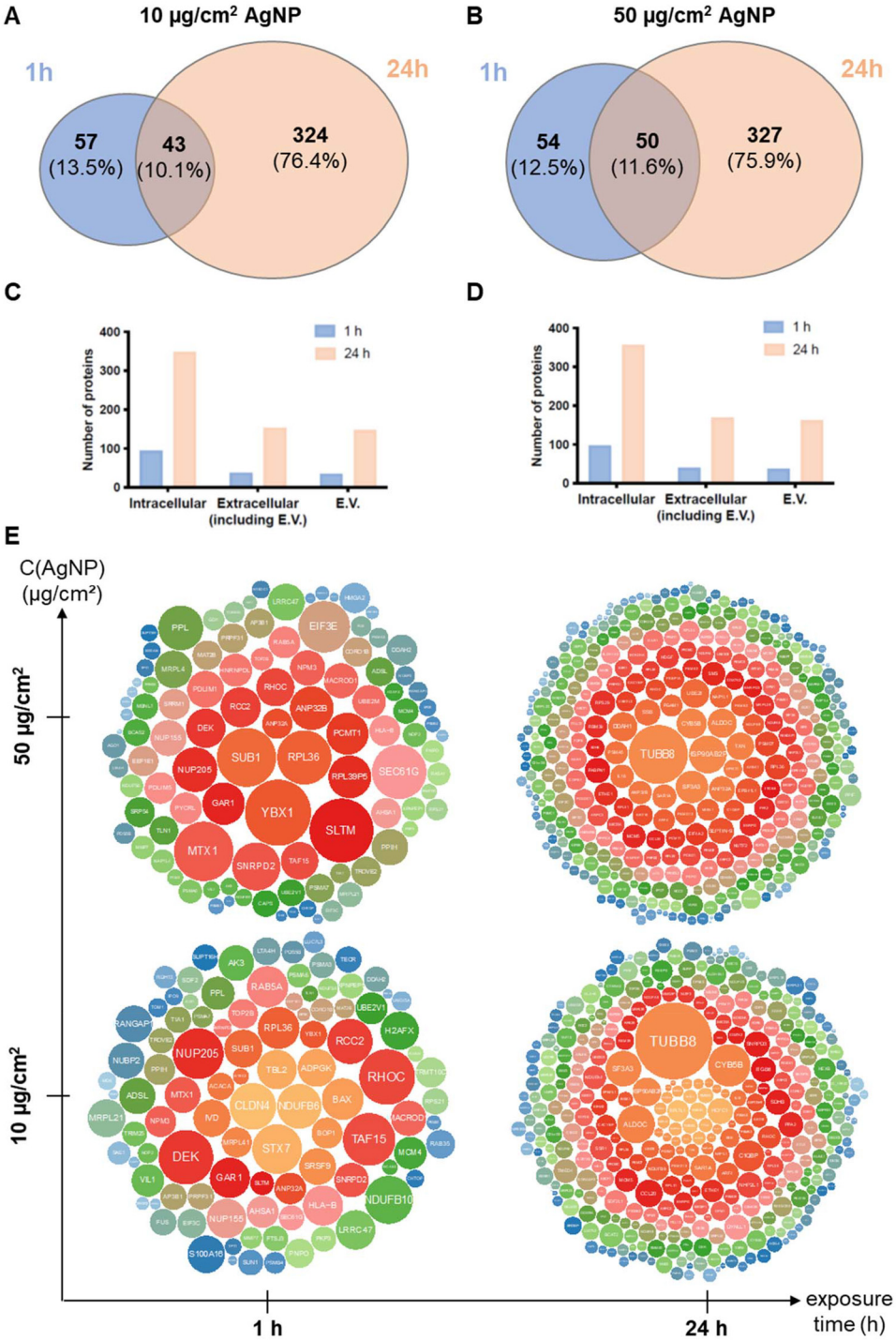

Fig. 3 Proteomic analysis of the cellular protein corona formed in the apical secretome during exposure of Calu-3 cells to AgNPs. (A and B) Venn diagram of protein corona composition after 1 and 24 h exposure to 10 or 50 μg cm^{-2} AgNPs. (C and D) Total number of intracellular proteins, extracellular proteins (including EV proteins), and proteins associated to extracellular vesicles. (E) Relative protein abundance as a function of AgNP concentration and exposure time.

were common to the cellular corona formed at the same exposure time at 10 and 50 μg cm^{-2} respectively (Fig. S3).

In the cellular corona, 40 and 170 proteins were classified as extracellular based on GO analysis, including the EV associated proteins after 1 h and 24 h exposure. It represents 29% and 32% of extracellular proteins, respectively (Fig. 3C and D). A similar ratio was observed for 10 and 50 μg cm^{-2} AgNPs. Cytosolic, organelle, membrane, exosomal, and extracellular proteins were identified in the protein corona in all the conditions. As cells were exposed to AgNPs at the ALI, no cell damage could occur due to mucus collection before a protein corona was formed. The presence of intracellular proteins in the corona suggests that they are naturally present in the mucus and originate from the natural renewal of the epithelium.

The relative abundance of the adsorbed proteins shows changes in the composition of the cellular corona both as a function of the exposure time and of AgNP concentration (Fig. 3E). The lists of the 10 most abundant proteins in each condition are provided in Tables S3 and S4. After 1 h exposure, the cellular corona was enriched in several RNA-binding proteins (TAF15, YBX1, SLTM, SUB1, and SNRPD2), lipid-binding proteins (STX7, CLDN4, SEC61G), and NADH-binding protein (NDUFB6, NDUFB10). After 24 h exposure, the cellular corona became enriched in chemokine 20 (CCL20) and C1q associated protein (C1QBP), two extracellular proteins involved in the epithelial inflammation and immune response that were absent in the corona at 1 h.

The Reactome pathway analysis shows a higher number of significantly enriched biological pathways in the cellular corona at 24 h compared to 1 h (Fig. S4), which is linked with the larger diversity of the protein corona at longer exposure time. A majority of the pathways are common to the cellular corona formed at 10 and 50 μg cm^{-2}. At 1 h, the main biological pathway identified in the cellular corona is the metabolism of RNA (24 and 25 proteins). This pathway becomes more enriched after 24 h exposure with 57 proteins identified in the cellular corona. The biological pathways specific to the long exposure time of Calu-3 cells include the metabolism of proteins (117 proteins) and protein translation (45 proteins). The same number of proteins were identified for these pathways after 24 h at 10 and 50 μg cm^{-2}. The NF-κB signalling was enriched in the cellular corona at 24 h (18 and 19 proteins) at both concentrations, while it was enriched at 1 h at 50 μg cm^{-2} AgNPs only, suggesting that local cytotoxicity effects may be reflected in the composition of the cellular corona.

To conclude this part, major reshuffling of the protein corona with exposure of Calu-3 cells to AgNPs was observed through a 3-fold increase in protein diversity and by change in both the relative protein abundance and functional protein network.

The response of epithelial cells shapes the corona of AgNPs

We compared the composition of the acellular and cellular protein corona after incubation in the bronchial mucus or exposure of Calu-3 cells for 1 h (Fig. 4A and B). Only 6% and 9% of the proteins were common to the acellular and cellular protein corona at 10 and 50 μg cm^{-2}, demonstrating the major role of cell exposure in the formation of the corona. At low NP concentration, 63 proteins were specific to the acellular protein corona, while 90 proteins were specific to the cellular protein corona. At high NP concentration, 74 proteins were specific to the acellular protein corona, while 88 proteins were specific to the cellular protein corona.

A heat map of the 10 most abundant proteins highlights the major differences in protein composition and relative abundance between the acellular and cellular protein corona (Fig. 4C). Several proteins highly enriched in the cellular corona are missing in the acellular corona, while some proteins enriched in the acellular corona are lacking in cellular conditions. Despite the incubation of the same NPs in the same initial biological medium, major differences are thus observed in the formation of the protein corona *in situ* during cell exposure.

This analysis could not be performed at 24 h due to the fast enzymatic degradation of some proteins in the mucus during incubation at 37 °C in the absence of protease inhibitors. However, our results demonstrate that even after 1 h exposure, when protein corona diversity is not yet maximized under cellular conditions, the compositions differ significantly between coronas formed in bronchial mucus with and without cell exposure.

Cell secretory mechanisms remodel the nano/bio interface

We monitored the cellular response of Calu-3 cells after exposure to 10 and 50 μg cm^{-2} AgNPs for 1 h, 24 h, and 48 h to further explore the connection between cell exposure, protein secretion, and the formation of the protein corona *in situ*. We quantified the mRNA expression of interleukins 6 and 8 (*il6*, *il8*), heme oxygenase (*hmox-1*), metallothioneins (*mt1x*, *mt2a*), albumin (*alb*), and mucine 5AC (*muc5ac*) as markers of the pro-inflammatory, antioxidant, metal detoxification, stress response, and the production of gel-forming mucin respectively (Fig. 5A–G).

After 1 h exposure, we observed a significant and concentration-dependent increase of *hmox-1*, *mt1x*, and *mt2a* gene expression corresponding to the antioxidant and metal detoxification pathways. This induction was no longer observed after 24 h and 48 h exposure to low AgNP concentration, while overexpression was observed only at 48 h at high AgNP concentration, suggesting cellular adaptation to AgNP pro-oxidant and metallic stress effects. A concentration-dependent downregulation trend of *alb* expression suggests a stress response of the epithelial cells,[75] albeit not significant in our conditions.

No significant increase of *il6*, *il8*, and *muc5ac* expression were observed. The secretion of IL-6 and IL-8 cytokines was measured in the apical secretome by ELISA assays (Fig. 5H and I). AgNPs induced a significant increase of IL-6 and IL-8 secretion after 24 and 48 h exposure compared to the control, but not after 1 h. These results suggest that the pro-inflammatory response was induced at the mRNA level between 1 and 24 h. The secretion of cytokines in the apical secretome during

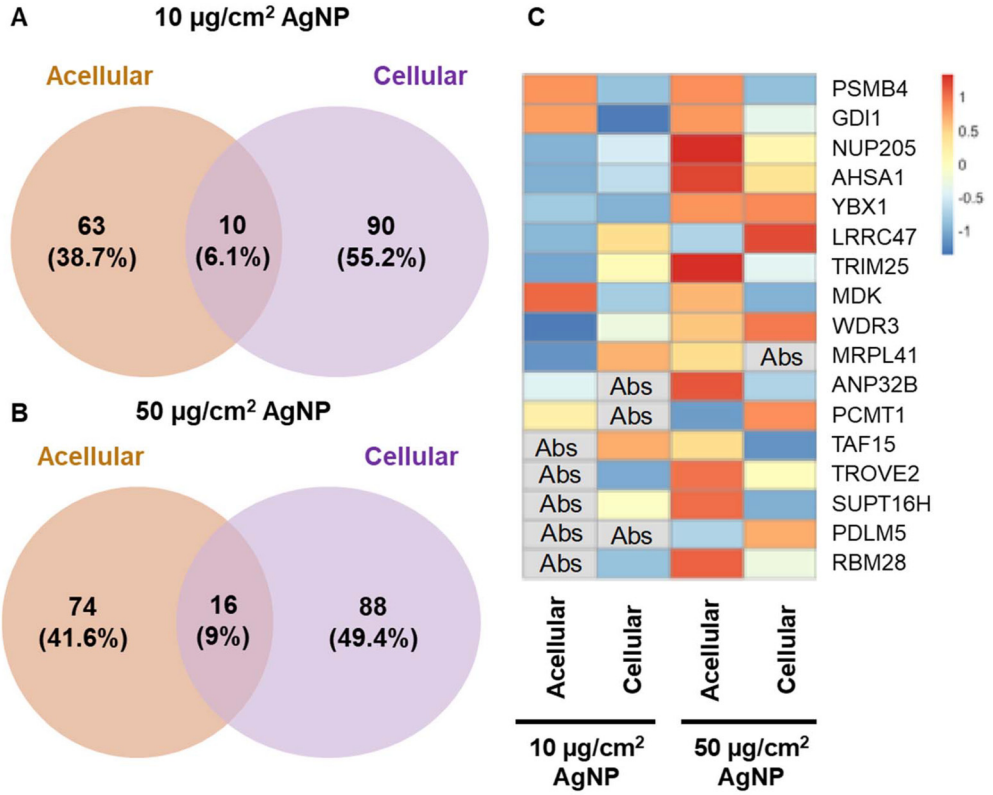

Fig. 4 Comparison of the NP protein corona formed in the apical secretome of Calu-3 cells with and without direct cell exposure to AgNPs. (A and B) Venn diagram of the composition of the protein corona in acellular and cellular condition for 10 and 50 µg cm^{-2} AgNPs after 1 h incubation or exposure. (C) Heat map of the 10 most abundant proteins in each condition. Abs: not present in the corona.

cell exposure to AgNPs represents a single change in the composition of the mucus where the protein corona forms.

To complete this analysis, the composition of the apical secretome of untreated and treated cells was compared based on published datasets.[59] Calu-3 cells were exposed to 50 µg cm^{-2} AgNPs at the ALI for 48 h, and control cells were exposed to HBSS. The apical secretome of control and treated cells shared 527 common proteins (84%) (Fig. 5J). 94 proteins (15%) were unique to cells exposed to AgNPs, while 12 proteins (2%) were expressed or detected in control cells only.[59]

To take into account changes in protein abundance, the data are visualized in a Volcano plot to identify proteins with statistically significant overexpression or underexpression in the secretome of Calu-3 cells exposed to AgNPs relative to the control (Fig. 5K). 9 proteins were significantly overexpressed in treated cells ($\log_2$ fold change > 1 and $-\log_{10} P > 1.5$), while 1 protein was significantly underexpressed ($\log_2$ fold change < −1 and $-\log_{10} P > 1.5$). AgNPs enhanced the secretion of 8 proteins that can be associated with extracellular exosomes (Table S5) such as adenylyl cyclase-associated protein 1 (CAP1) and glyceraldehyde-3-phosphate dehydrogenase (GAPDH).[76]

Finally, we used this dataset to compare the compositions of the apical secretome of Calu-3 exposed to AgNPs with the protein corona formed *in situ*. For this analysis, we focused on proteins uniquely expressed in the secretome of treated cells only to determine whether the cellular response to AgNPs can directly influences the biomolecular corona formation. The exposure time differed between datasets (24 h for the protein corona *versus* 48 h for the secretome) but the use of identical cellular models, AgNP concentrations, and exposure conditions provides a good first step to compare both datasets. Our analysis identified 20 proteins present in both the apical secretome of AgNP-exposed cells and the protein corona formed *in situ* (Table S6). This finding provides evidence that the cellular response to NP exposure contributes to the formation of the corona, demonstrating a dynamic interplay between cellular secretory mechanisms and the nano/bio interface.

Discussion

Quantitative proteomic analysis of the biomolecular corona formed on AgNPs in cell-free bronchial mucus and during exposure of Calu-3 cells to AgNPs revealed major changes in both protein nature and abundance. The protein corona formed *in situ* contains unique proteins and is richer and more diverse than that formed in bronchial mucus collected from untreated Calu-3 cells, demonstrating how exposure to

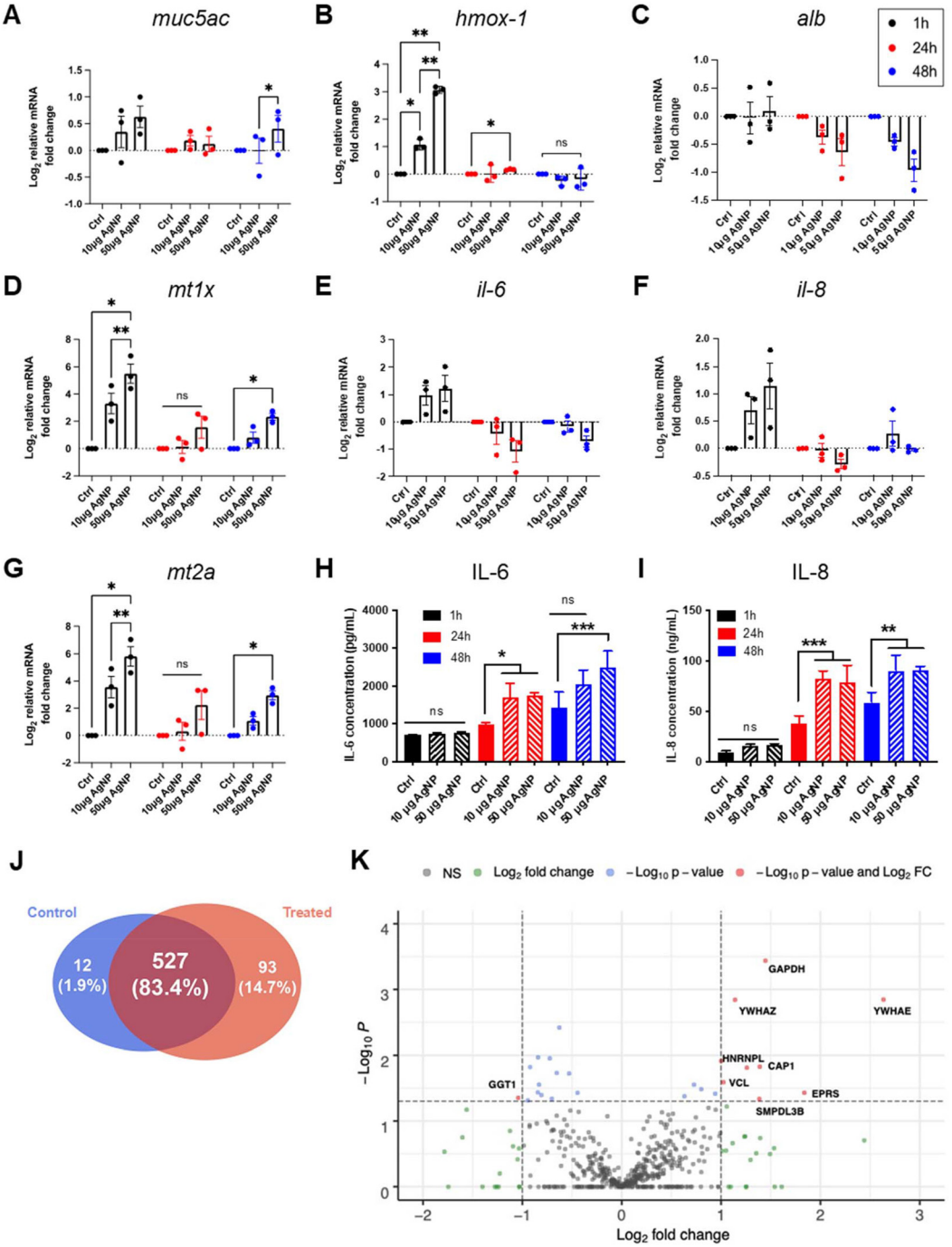

Fig. 5 Cellular response of Calu-3 cells exposed to 10 and 50 µg cm^{-2} AgNPs at ALI for 1 h, 24 h, and 48 h. (A–G) mRNA expression of mucin 5AC (*muc5ac*), heme oxygenase (*hmox-1*), albumin (*alb*), metallothioneins (*mt1x*, *mt2a*), interleukins 6 and 8 (*il6*, *il8*). (H–I) Concentration of IL-6 and IL-8 in the apical secretome. (J) Venn diagram of the composition of the apical secretome of control cells and cells exposed to 50 µg cm^{-2} AgNPs for 48 h, adapted from.[59] (K) Volcano plot of the composition of the protein corona and the apical secretome of Calu-3 cells exposed to 50 µg cm^{-2} AgNPs. Data are presented as $\log_2$ fold change *versus* $-\log_{10} p$-value. Significantly over- or underexpressed proteins are highlighted in red. NS: non-significant.

AgNPs induces cellular pathways in epithelial cells that modify the protein corona.

The increase in the number of proteins in the corona after 24 h exposure of Calu-3 cells compared to 1 h illustrates the time scale of the cell response. Because differentiated cells do not proliferate in the 3D model, they form a stable epithelium for the analysis of the cellular response *in vitro* without interference from the cell cycle. While it is well known that the

protein corona evolves with the incubation time in a biological fluid, such as plasma or serum, due to differences in protein affinity for the NP surface and structural changes, few studies have reported the evolution of the protein corona during cell exposure. Based on our results, we can propose that the following stages occur:

(a) AgNP deposition in the airways;

(b) AgNP diffusion into the mucus layer;

(c) Direct or indirect interaction of AgNPs with the apical membrane of epithelial cells;

(d) Cellular response to AgNPs exposure;

(e) Remodeling of the corona by protein adsorption/desorption.

Each step is described and discussed in more detail below:

(a) In an inhalation scenario, AgNPs are transported by airflow to the bronchi and alveoli where they can be deposited depending on their hydrodynamic diameter, shape and density. The NPs are thus free of any biomolecule and maintain a pristine or environmental surface until they are deposited in the airways. This step corresponds to the time t_0.

(b) Bronchial mucus is a viscoelastic gel network of cross-linked mucins with pore sizes ranging from tens to hundreds of nm. The diffusion of NPs in mucus is well documented in the literature for drug delivery applications using various mucus models, including the apical secretome of Calu-3 cells.[77] The effective diffusion coefficient of polymeric NPs in the respiratory mucus varies from tens to thousands of times lower values compared to diffusion in water.[78,79] It depends on the size, shape and surface charge of the NPs and on the viscoelastic properties of the mucus sample used for analysis. The diffusivity and mean squared displacements of particles in mucus also depend on their coating.[80] Pre-coating with BSA can increase the mobility of NPs across the mucus barrier compared to bare particles. This suggests that changes in the composition or structure of the protein corona may alter NP diffusion through the mucus layer, allowing more particles to come into contact with epithelial cells.

As protein adsorption is a rapid process, we hypothesise that an initial protein corona forms on contact with bronchial mucus before any cellular response alters the cell microenvironment. This protein corona would be identical to the protein corona formed in bronchial mucus collected from control cells. It could evolve as a function of protein distribution within the mucus layer, differences in protein affinity for the surface, and structural changes in the adsorbed proteins.

(c) Direct interaction of AgNPs with Calu-3 cells refers to endocytosis or binding to the outer apical membrane of the cell. This mechanism can be non-specific or specific if proteins in the corona bind to membrane receptors.[18] Interactions with microvilli are also possible. The observation of AgNPs in the cytoplasm of Calu-3 cells reported in[59] suggests that direct interaction and endocytosis of AgNPs occurred, albeit on a small scale. Indirect interactions refer to the release of silver ions by AgNPs and the production of reactive oxygen species through chemical and biochemical reactions within the mucus layer. SAXS data show that AgNPs are stable in the bronchial mucus with little or no dissolution observed.

(d) The cellular response to AgNPs involves the activation of intracellular pathways to counteract the toxic effects of silver in particulate or ionic form. Overexpression of metallothioneins is required for silver ion sequestration and detoxification, an indicator of partial dissolution of AgNPs in cells. Superoxide dismutase and heme oxygenase protect cells from ROS by catalysing the dismutation of superoxide anion and the degradation of heme, respectively. Other intracellular pathways not investigated in this study are likely to be involved in the cellular response to AgNPs, as documented in other studies using whole genome transcriptomic analysis.[81] The proteomic analysis of the apical secretome of exposed cells reported in ref. 59 provides additional information on the secretory machinery of Calu-3 cells. Several proteins are secreted into the extracellular space, either freely or as extracellular vesicles. These proteins may be involved in cell–cell communication, immune response and inflammatory response between airway epithelial cells.[72]

Inhalation of AgNPs has been reported in occupational epidemiologic studies. Exposure to AgNPs in a manufacturing facility was estimated to 1.35 μg m^{-3}. Higher concentrations of 5 to 290 μg m^{-3} have been measured during the production step of AgNPs.[82] Absorption of silver by inhalation or other routes in exposed workers resulted in blood concentrations ranging from 6 to 74 μg(Ag) L^{-1}, with the highest concentration of 154 μg(Ag) L^{-1} measured in a 27 year-old man exposed to aerosolised silver.[63] These data confirm that a fraction of inhaled AgNPs is translocated to the blood, either at the bronchial or alveolar level.

(e) These different steps may occur sequentially or, more likely, in an overlapping time frame. The evolution of the protein corona between 1 h and 24 h exposure suggests that the cellular response has started before 1 h (the protein corona is different from that formed in acellular bronchial mucus), but is more prominent between 1 h and 24 h. The kinetics of the cellular detoxification process is likely to depend on the concentration, composition and pathways activated by a particular NP. Typical timescales for detoxification pathways in eukaryotic cells range from a few minutes for the initial enzymatic response, to several hours and up to several days for cell adaptation,[83] which is consistent with our results.

Several exosomal proteins were identified in the apical secretome of Calu-3 cells exposed to AgNPs for 48 h. Since these proteins were absent from the apical secretome of control cells, we conclude that they are part of the secretory response of Calu-3 cells to NP exposure. The same proteins were identified in the biomolecular corona formed *in situ*, confirming that they were already secreted after 24 h exposure of Calu-3 cells to AgNPs. Adsorption on AgNPs shows that these exosomal proteins have a strong affinity for the NP surface. Other exosomal proteins produced by the cells may not be present in the corona. It is likely that exosomes secreted by Calu-3 cells exposed to AgNPs come into contact with the particles trapped in the mucus layer, leading to destabilization of

the exosomes or extracellular vesicles and protein exchange with AgNPs.[84] Other possible mechanisms include internalization of AgNPs and subsequent release of NP-loaded exosomes, or binding of AgNPs to the outer membrane where EVs would form. To our knowledge, very little is known about the relationship between exosomes and NPs. A dedicated study of EVs in bronchial mucus from cells exposed to AgNPs may help to elucidate their specific role in mediating the epithelial cell response to toxic particles.

Internalization of AgNPs by Calu-3 cells after repeated exposure for 12 days at ALI was shown by TEM on thin sections after cell fixation.[59] Less than 0.2% of the silver translocated to the basal compartment, either in particulate or ionic form, while an increased silver concentration in the mucus suggested that AgNPs accumulated in the mucus layer. In a co-culture model of Calu-3 epithelial cells, THP-1 macrophages and endothelial cells, the combined silver uptake of Calu-3 and THP-1 cells was estimated to 9% after a single exposure of 24 h at ALI.[85] These data suggest that AgNPs remaining in the mucus, as observed in the TEM images in this study, represent the majority of particles delivered to the bronchi, where they become available for mucociliary clearance and cellular interactions with resident macrophages. Therefore, analysis of the protein corona in bronchial mucus is relevant for assessing the toxicity and fate of inhaled AgNPs. The analysis of the interaction between macrophages and AgNPs covered by a cellular biomolecular corona is a direct perspective of this study.[67]

We termed the biomolecular corona formed by the epithelial response to NP exposure the 'cellular corona' in contrast to the 'acellular corona' formed only in cell-free bronchial mucus. However, the composition of the intracellular protein corona of AgNPs after uptake by epithelial cells remains a blind spot. Recycling of the protein corona into endosomes has been demonstrated in murine RAW264.7 macrophages using fluorescently labelled plasma proteins and polystyrene NPs.[86] A previous study using a similar approach observed only partial degradation of the protein corona, with some proteins retained on polystyrene NPs in the lysosome of alveolar A549 cells.[30] While fluorescent labelling provides high sensitivity for the detection and localization of proteins in cells, it alters the composition of the protein corona[86] and does not provide information on the newly formed intracellular corona. If the protein corona is partially or completely degraded, other mechanisms may be at work at the nano/bio interface, such as NP-membrane interactions.[87] In the case of AgNPs, the dissolution kinetics of silver, especially in more acidic lysosomes, is a competing mechanism that may further destabilise the interface at the molecular level.

The formation of the protein corona has been reported in isolated pulmonary fluids, in bronchial alveolar lavage from humans or small animals, and for different lung cell lines.[8,30,49,88,89] The advantage of the 3D model of the bronchial epithelium at ALI is that it combines the cellular and barrier functions of the epithelial cells together with the production of a mature mucus layer on the apical side. Analysis of the protein corona formed *in situ* using a 3D model of the bronchial epithelium provides a more realistic and accurate description of corona formation after NP inhalation. Although cells do not actively construct the corona on NPs, the cellular pathways and biochemical changes induced by the exposure to AgNPs modify its composition.[25] This effect depends on the intracellular localization and fate of NPs in a specific cell or tissue.[90] Very few studies have investigated the formation of the protein corona in pulmonary fluids. This methodology could be applied in future work at the alveolar level, such as in co-culture of type I and type II pneumocytes,[66] to complete the knowledge of the interplay between cellular response and adsorption of biomolecules on inhaled particles or fibres.

Experimental

Chemicals

AgNPs were provided by the European Commission Joint Research Centre (NM300K, JRC). NM300K is a reference manufactured nanomaterial.[68] AgNPs are spherical with an average TEM diameter of 17 ± 8 nm with smaller NPs < 5 nm present. The aqueous suspension has a nominal Ag concentration of 10% w/w and is stabilized with 4% w/w polyoxyethylene glycerol trioleate and polyoxyethylene 20 sorbitan monolaurate (Tween 20). AgNP stock suspension was diluted to 1 mg mL^{-1} in Hanks' Balanced salt solution (Gibco, France) supplemented with Ca^{2+} and Mg^{2+} ($HBSS^{Ca^{2+}/Mg^{2+}}$) and sonicated 2 × 2 min on ice with a cup horn sonicator (450 W, 60 Hz, Branson).

Characterization of AgNPs

The diameter of AgNPs in the stock suspension was measured by TEM. The suspension was diluted to 0.5 mg mL^{-1} in milliQ water and a drop was deposited and dried on Cu–C–Formvar grid. The images were acquired at 80 kV on a Jeol JEM-100S microscope (Jeol Ltd Tokyo, Japan) equipped with an Orius 200 digital camera (Gatan-Roper Scientific, France). The images were analyzed with ImageJ software to determine the average diameter of AgNPs. A total number of 2500 particles were analyzed. Results are expressed as mean ± standard deviation.

The hydrodynamic diameter of AgNPs in $HBSS^{Ca^{2+}/Mg^{2+}}$ was measured by DLS. AgNPs were diluted to 0.01 mg mL^{-1} in $HBSS^{Ca^{2+}/Mg^{2+}}$ and incubated for 1 h at 37 °C. The hydrodynamic diameter was measured on a Zetasizer (Malvern, UK). It is expressed as mean ± standard deviation of 3 independent replicates.

The diameter and stability of AgNPs in the apical secretome of Calu-3 cells was measured by SAXS. AgNPs were diluted to 0.5 mg mL^{-1} in the secretome of mature Calu-3 cells for 1, 24, and 48 h at 37 °C. The secretome was incubated in the same condition without AgNPs as a control. 50 μL of the suspension was transferred to a kapton capillary and analyzed on a Xeuss 2.0 high resolution X-ray spectrometer (Xenocs, France). The signal was acquired for 3600 s for each sample. The capillaries

were measured at different y-positions along the vertical axis during the experiment. Two replicates were analyzed for each condition. After subtraction of the background signal, SAXS data were fitted with a Gaussian polydisperse sphere model using the following parameters: ρ_{Ag} = 10.5 g cm^{-3}, scattering length density $SLD_{water} = 9.39 \times 10^{-10}$ cm^{-2} and $SLD_{Ag} = 7.76 \times 10^{-11}$ cm^{-2}. The particle size distribution and concentration (in number per mL) were calculated by curve fitting of SAXS data using a monodisperse sphere model. Data are expressed as mean ± standard deviation.

3D model of human bronchial epithelium

Calu-3 human adenocarcinoma epithelial cells (ATCC® HTB-55™, LGC standard, France) were used from passage 27 to 34. The protocol for Calu-3 cell culture and differentiation at ALI was described in our previous study.[52] Briefly, Calu-3 cells were seeded on Millicell® porous inserts (Millipore, Sigma, France) in MEM supplemented with 10% FBS (F7524, Sigma, France). The surface area of each insert is 1.1 cm^2 and the pore diameter is 3 μm. When Calu-3 cells reached a transepithelial electric resistance (TEER) of 700 Ω cm^2, the apical medium was removed to induce ALI. The concentration of serum in the basolateral medium was reduced to 4% FBS one day after ALI. Cultures were maintained in ALI for 10 days to obtain a mature secretome.[52]

Formation of the acellular protein corona

AgNP stock suspension was first diluted to 0.5 or 2.5 mg mL^{-1} in $HBSS^{Ca^{2+}/Mg^{2+}}$ buffer and sonicated 2 × 2 min on ice. 20 μL of AgNP diluted suspension were mixed with the apical secretome of the mature bronchial epithelium collected at ALI in 200 μL $HBSS^{Ca^{2+}/Mg^{2+}}$. The acellular protein corona was formed by incubating 10 or 50 μg AgNPs in 200 μL of apical secretome for 1 h at 37 °C under gentle mixing. Samples were stored at −80 °C before analysis.

Exposure of Calu-3 cells to AgNPs

The apical secretome was collected 12 h before starting the treatment. Calu-3 cells were exposed to 10 or 50 μg cm^{-2} AgNPs at ALI for 1 h and 24 h for the analysis of the cellular corona, and for 1 h, 24 h, and 48 h for toxicity endpoints. AgNP stock suspension was first diluted to 0.5 or 2.5 mg mL^{-1} in $HBSS^{Ca^{2+}/Mg^{2+}}$ buffer and sonicated 2 × 2 min on ice. 20 μL of AgNP diluted suspension were deposited on the apical side of Calu-3 cells at ALI as 4 drops of 5 μL each. Following exposure, the mucus layer containing AgNPs was collected in 200 μL $HBSS^{Ca^{2+}/Mg^{2+}}$. Control cells were treated with the same volume of HBSS. Samples were stored at −80 °C before analysis.

Toxicity endpoints

The epithelial barrier integrity was monitored by measuring the TEER and the Lucifer Yellow paracellular permeability. The TEER was measured with an EVOM2 ohmmeter (World Precision Instrument, USA) equipped with an STX2 electrode after replacing the culture medium by $HBSS^{Ca^{2+}/Mg^{2+}}$. The Lucifer Yellow (LY) permeability was measured by fluorescence after incubation of 0.5 mL of LY dye in the apical compartment for 1 h at 37 °C. The fluorescence intensity of LY in the basal medium was measured in $HBSS^{Ca^{2+}/Mg^{2+}}$ on a microplate reader (Flexstation 3, Molecular Devices) using an excitation and an emission wavelength of 485 and 535 nm.

The metabolic activity was measured using the Alamar Blue assay, which is based on resazurin reduction to resorufin by metabolically active cells. Cells were incubated with the reagent for 1 h at 37 °C. The fluorescence intensity of resorufin in the basal medium was measured in $HBSS^{Ca^{2+}/Mg^{2+}}$ on a microplate reader using an excitation and an emission wavelength of 545 and 590 nm. No interference with AgNPs was observed.

The secretion of interleukin-6 (IL-6) and interleukin-8 (IL-8) pro-inflammatory cytokines was quantified in the apical and basal media by ELISA assays (DuoSet ELISA kit, R&D Systems, France). The absorbance at 490 nm was measured on a microplate reader.

The gene expression of cytokines *il6* and *il8*, heme oxygenase *hmox-1*, metallothioneins *mt1x* and *mt2a*, mucin *muc5ac*, and albumin *alb*, was quantified by RT-qPCR. The sequence of the primers is detailed in Table S1. RNA was extracted using the NucleoSpin® kit (Macherey-Nagel, France) and reverse transcribed using High-capacity cDNA Reverse Transcription kit (Thermo Fisher, France). Reactions were carried out in sealed 384-well plates in a LightCycler 480 thermocycler (Roche Diagnostics, France). Gene expression was quantified using $2^{-\Delta\Delta Ct}$ method to yield $\log_2$ fold change of a gene relative to *rpl19* as housekeeping gene and normalized to the control.

Isolation of AgNPs in the bronchial mucus

AgNPs were separated from free proteins in solution by centrifugation at 3000*g* for 20 min at 4 °C followed by 3 washes in $HBSS^{Ca^{2+}/Mg^{2+}}$ and centrifugation at 14 000*g* for 20 min at 4 °C (Fig. S1A). We adapted the protocol to isolate the protein corona of AgNPs in the bronchial mucus to avoid the precipitation of free proteins during centrifugation.[70] The apical secretome is a viscous medium composed of high molecular weight proteins that tend to sediment if a standard protocol for NP separation by centrifugation is applied. Freeze/thaw cycle at −80 °C followed by a low-speed centrifugation reduced the precipitation of free proteins. Supernatants and washes were analyzed by standard SDS-PAGE. The same isolation protocol was applied to the apical secretome of control and treated cells.

Proteomics

After isolation of AgNPs from the mucus, the protein corona was extracted by SDS-PAGE using a short migration time to concentrate the desorbed proteins in one large band. Proteins were treated in the gel with dithiothreitol and iodoacetamide (Sigma, France) and digested with trypsin (Trypsin Gold V5280, Promega, France). The peptides were extracted from the gel and rinsed using Pierce® C18 tips (Thermo Fisher, France) following manufacturer's instructions. The protocol for AgNP

isolation by centrifugation was applied to the apical secretome of untreated cells as a control to exclude false positive. The pellet was digested using the same protocol and analyzed by LC-MS/MS to identify free proteins that sedimented without AgNPs. The proteins identified were excluded from the protein list of the corona.

The peptides from the protein corona and control samples were analyzed by LC-MS/MS on an Orbitrap Fusion Tribrid mass spectrometer following the protocol described by Soliman *et al.*[91] Peptide and protein identification were performed with MaxQuant software and Andromeda peptide search engine using a mass tolerance of 10 ppm and a fragment tolerance of 0.5 Da.[92] The *Homo sapiens* and *Bos Taurus* RefSeq databases from the NCBI were used to identify proteins based on the peptide sequence with a maximum of 2 missed cleavages. A false positive discovery rate of 0.01 was chosen for both peptides and proteins. MaxLFQ algorithm was used to extract normalized semi-quantitative data for each protein (relative abundance). The functional analysis of the quantitative proteomic datasets was done using Perseus bioinformatics platform.[93] The results are presented using R software (v. 3.6.2) implemented with pheatmap and packcircles packages.[94] Gene ontology and functional enrichment analysis were performed with g:Profiler and g:GOSt implemented with g:SCS.[95] A threshold of 0.05 was applied to the results.

Statistical analysis

The statistical analysis was performed with Prism GraphPad Software (v. 7.0). Results are expressed as mean ± standard error of 3 independent replicates. Normality was tested using Agostino and Pearson or the Shapiro–Wilk test with $a = 0.05$. When comparing groups, two-way ANOVA corrected with Benjamini, Krieger and Yekutieli test was applied. When comparing time variability within a group, three-way ANOVA corrected with Benjamini, Krieger and Yekutieli test was applied. The Bonferroni-Dunn *t*-test method was applied to LY permeability data. *P*-values < 0.05 were considered as statistically significant. For Volcano plot, a threshold of $\log_2$ fold change >1 or <1 and $-\log_{10} P > 1.5$ was defined to identify overexpressed and underexpressed proteins.

Conclusion

This study demonstrates the role of the epithelial cell response in the formation and composition of the protein corona on silver nanoparticles. The marked difference in composition between the corona formed in the bronchial mucus without cells and *in situ* during cell exposure to NPs calls for a renewed focus on the role of cells and cell-NP interaction in biomolecular corona studies. It encourages the community to develop innovative methods to analyse molecular mechanisms such as protein adsorption and structural changes in a more complex living cell environment. The rapid development of omics technologies and advanced 3D cell models, from co-cultures in fluidic devices to functional organoids, can support these efforts without resorting to animal testing to better understand the molecular and cellular mechanisms of NP toxicity.

Author contributions

D. S. G. performed the experiments and analyzed the data. C. C., O. T., and M. P. M. contributed to the experiments. D. S. G. and S. D. analyzed the proteomic data. S. D., A. B. S. and D. S. G. designed the study. S. D. and D. S. G. wrote the manuscript. All authors reviewed the manuscript.

Conflicts of interest

There are no conflicts to declare.

Abbreviations

ALI	Air–liquid interface
AgNP	Silver nanoparticle
BALF	Bronchoalveolar lavage fluid
DLS	Dynamic light scattering
EV	Extracellular vesicles
HBSS	Hank's balanced salt solution
NHBE	Normal human bronchial epithelial
NOAEC	No observed adverse effect concentration
NP	Nanoparticle
RTLF	Human respiratory tract lining fluid
SAXS	Small angle X-ray scattering

Data availability

The mass spectrometry proteomics data have been deposited to the ProteomeXchange Consortium *via* the PRIDE partner repository with the dataset identifier PXD063611 and are available at **https://www.ebi.ac.uk/pride/**.

Supplementary information (SI): full list of proteins identified by mass spectrometry is included in the Excel file. See DOI: **https://doi.org/10.1039/d5nr02590g**.

The other datasets are available from the corresponding author upon request.

Acknowledgements

The authors thank Duong N. Trinh, RCSI, for her assistance with sample preparation. This project received funding from the European Union's Horizon 2020 research and innovation program under grant agreement no. 760928 (BIORIMA). DSG was supported by a fellowship from the Ecole Doctorale MTCI, Université Paris Cité.

References

1 M. Abrami, A. Biasin, F. Tescione, D. Tierno, B. Dapas, A. Carbone, G. Grassi, M. Conese, S. Di Gioia, D. Larobina and M. Grassi, *Int. J. Mol. Sci.*, 2024, **25**, 1933.
2 M. P. Monopoli, C. Aberg, A. Salvati and K. A. Dawson, *Nat. Nanotechnol.*, 2012, **7**, 779–786.
3 M. Falahati, A. Hasan, H. A. Zeinabad, V. Serpooshan, J. H. von der Thüsen and T. L. M. ten Hagen, *Nano Today*, 2023, **52**, 101998.
4 A. Aliyandi, C. Reker-Smit, R. Bron, I. S. Zuhorn and A. Salvati, *ACS Biomater. Sci. Eng.*, 2021, **7**, 5573–5584.
5 L. Zhang, T. Sun, M. Gong, C. Zhou, Y. Zhao, W. Zhang, Z. Zhang, S. Xiao, X. Yang, M. Wang, X. Liu, Q. Xie and D. Zhang, *Mater. Today Bio*, 2024, **28**, 101215.
6 Y. Miao, L. Li, Y. Wang, J. Wang, Y. Zhou, L. Guo, Y. Zhao, D. Nie, Y. Zhang, X. Zhang and Y. Gan, *Nat. Commun.*, 2024, **15**, 1159.
7 L. Papafilippou, A. Nicolaou, A. C. Kendall, D. Camacho-Muñoz and M. Hadjidemetriou, *Nanoscale*, 2023, **15**, 11038–11051.
8 S. S. Raesch, S. Tenzer, W. Storck, A. Rurainski, D. Selzer, C. A. Ruge, J. Perez-Gil, U. F. Schaefer and C.-M. Lehr, *ACS Nano*, 2015, **9**, 11872–11885.
9 A. Lesniak, F. Fenaroli, M. P. Monopoli, C. Åberg, K. A. Dawson and A. Salvati, *ACS Nano*, 2012, **6**, 5845–5857.
10 C. D. Walkey, J. B. Olsen, F. Song, R. Liu, H. Guo, D. W. H. Olsen, Y. Cohen, A. Emili and W. C. W. Chan, *ACS Nano*, 2014, **8**, 2439–2455.
11 C. Corbo, R. Molinaro, A. Parodi, N. E. Toledano Furman, F. Salvatore and E. Tasciotti, *Nanomedicine*, 2016, **11**, 81–100.
12 Y.-t. Li, K.-C. Mei, R. Liam-Or, J. T.-W. Wang, F. N. Faruqu, S. Zhu, Y.-l. Wang, Y. Lu and K. T. Al-Jamal, *ACS Nano*, 2024, **18**, 22572–22585.
13 R. Bilardo, F. Traldi, A. Vdovchenko and M. Resmini, *Nanomed. Nanobiotechnol.*, 2022, **14**, 1–22.
14 M. Mahmoudi, M. P. Landry, A. Moore and R. Coreas, *Nat. Rev. Mater.*, 2023, **8**, 422–438.
15 S. Li, C. Cortez-Jugo, Y. Ju and F. Caruso, *ACS Nano*, 2024, **18**, 33257–33263.
16 P.-L. Latreille, M. Le Goas, S. Salimi, J. Robert, G. De Crescenzo, D. C. Boffito, V. A. Martinez, P. Hildgen and X. Banquy, *ACS Nano*, 2022, **16**, 1689–1707.
17 G. Caracciolo, O. C. Farokhzad and M. Mahmoudi, *Trends Biotechnol.*, 2017, **35**, 257–264.
18 S. Lara, F. Alnasser, E. Polo, D. Garry, M. C. Lo Giudice, D. R. Hristov, L. Rocks, A. Salvati, Y. Yan and K. A. Dawson, *ACS Nano*, 2017, **11**, 1884–1893.
19 M. Aoyama, K. Hata, K. Higashisaka, K. Nagano, Y. Yoshioka and Y. Tsutsumi, *Biochem. Biophys. Res. Commun.*, 2016, **480**, 690–695.
20 S. Linse, C. Cabaleiro-Lago, W.-F. Xue, I. Lynch, S. Lindman, E. Thulin, S. E. Radford and K. A. Dawson, *Proc. Natl. Acad. Sci. U. S. A.*, 2007, **104**, 8691–8696.
21 C. Pisani, E. Rascol, C. Dorandeu, J.-C. Gaillard, C. Charnay, Y. Guari, J. Chopineau, J. Armengaud, J.-M. Devoisselle and O. Prat, *PLoS One*, 2017, **12**, 1–17.
22 C. Mathé, S. Devineau, J.-C. Aude, G. Lagniel, S. Chédin, V. Legros, M.-H. Mathon, J.-P. Renault, S. Pin, Y. Boulard and J. Labarre, *PLoS One*, 2013, **8**, 1–13.
23 Q. Hu, X. Bai, G. Hu and Y. Y. Zuo, *ACS Nano*, 2017, **11**, 6832–6842.
24 M. G. Soliman, A. Martinez-Serra, G. Antonello, M. Dobricic, T. Wilkins, T. Serchi, I. Fenoglio and M. P. Monopoli, *Environ. Sci.:Nano*, 2024, **11**, 4421–4448.
25 A. E. Nel, L. Mädler, D. Velegol, T. Xia, E. M. V. Hoek, P. Somasundaran, F. Klaessig, V. Castranova and M. Thompson, *Nat. Mater.*, 2009, **8**, 543–557.
26 J. Kobayashi, K. Higashisaka, M. Muranaka, Y. Xie, W. Okuno, Y. Haga and Y. Tsutsumi, *Biochem. Biophys. Res. Commun.*, 2024, **736**, 150488.
27 Y. Feng, H. Fu, X. Zhang, S. Liu and X. Wei, *Ecotoxicol. Environ. Saf.*, 2024, **286**, 117215.
28 Y. Arezki, E. Harmouch, F. Delalande, M. Rapp, C. Schaeffer-Reiss, O. Galli, S. Cianférani, L. Lebeau, F. Pons and C. Ronzani, *Int. J. Pharm.*, 2023, **645**, 123388.
29 R. Cai, J. Ren, M. Guo, T. Wei, Y. Liu, C. Xie, P. Zhang, Z. Guo, A. J. Chetwynd, P. C. Ke, I. Lynch and C. Chen, *Proc. Natl. Acad. Sci. U. S. A.*, 2022, **119**, 1–11.
30 F. Bertoli, D. Garry, M. P. Monopoli, A. Salvati and K. A. Dawson, *ACS Nano*, 2016, **10**, 10471–10479.
31 Z. Zhang, X. Dong, W. Wan, H. Guo, R. Sun, H. Feng, M. Wang, Z. Wang, H. Jin, J. Sun, Q. Xia, Q. Zhao, D. Shen, Z. Gao and Y. Liu, *Anal. Chem.*, 2024, **96**, 4978–4986.
32 M. Carril, D. Padro, P. del Pino, C. Carrillo-Carrion, M. Gallego and W. J. Parak, *Nat. Commun.*, 2017, **8**, 1542.
33 M. Martinez-Moro, D. Di Silvio and S. E. Moya, *Biophys. Chem.*, 2019, **253**, 106218.
34 G. P. Szekeres, M. Montes-Bayón, J. Bettmer and J. Kneipp, *Anal. Chem.*, 2020, **92**, 8553–8560.
35 M. C. Lo Giudice, L. M. Herda, E. Polo and K. A. Dawson, *Nat. Commun.*, 2016, **7**, 13475.
36 C. Wang, B. Chen, M. He and B. Hu, *ACS Nano*, 2021, **15**, 3108–3122.
37 W. Mekseriwattana, T. Thiangtrongjit, O. Reamtong, P. Wongtrakoongate and K. P. Katewongsa, *ACS Omega*, 2022, **7**, 37589–37599.
38 Y. Sun, Y. Zhou, M. Rehman, Y.-F. Wang and S. Guo, *Chem Bio Eng.*, 2024, **1**, 757–772.
39 L. Digiacomo, F. Giulimondi, M. Mahmoudi and G. Caracciolo, *Nanoscale Adv.*, 2019, **1**, 2518–2522.
40 P. L. Latreille, J. M. Rabanel, M. Le Goas, S. Salimi, J. Arlt, S. A. Patten, C. Ramassamy, P. Hildgen, V. A. Martinez and X. Banquy, *Adv. Mater.*, 2022, **34**, 1–14.
41 Y. Niu, Y. Yu, X. Shi, F. Fu, H. Yang, Q. Mu, D. Crespy, K. Landfester and S. Jiang, *Nano Lett.*, 2024, **24**, 9202–9211.
42 R. da Costa-Marques, N. Hüppe, K. R. Speth, J. Oberländer, I. Lieberwirth, K. Landfester and V. Mailänder, *Acta Biomater.*, 2023, **172**, 355–368.

43 A. Albanese, C. D. Walkey, J. B. Olsen, H. Guo, A. Emili and W. C. W. Chan, *ACS Nano*, 2014, **8**, 5515–5526.
44 M. Hadjidemetriou, S. McAdam, G. Garner, C. Thackeray, D. Knight, D. Smith, Z. Al-Ahmady, M. Mazza, J. Rogan, A. Clamp and K. Kostarelos, *Adv. Mater.*, 2019, **31**, 1–9.
45 Z. P. Lin, W. Ngo, S. M. Mladjenovic, J. L. Y. Wu and W. C. W. Chan, *Nano Lett.*, 2023, **23**, 1003–1009.
46 D. T. Jayaram, S. M. Pustulka, R. G. Mannino, W. A. Lam and C. K. Payne, *Biophys. J.*, 2018, **115**, 209–216.
47 J. Tan, A. Thomas and Y. Liu, *Soft Matter*, 2011, **8**, 1934–1946.
48 F. Giulimondi, L. Digiacomo, D. Pozzi, S. Palchetti, E. Vulpis, A. L. Capriotti, R. Z. Chiozzi, A. Laganà, H. Amenitsch, L. Masuelli, G. Peruzzi, M. Mahmoudi, I. Screpanti, A. Zingoni and G. Caracciolo, *Nat. Commun.*, 2019, **10**, 3686.
49 A. Kumar, E. M. Bicer, A. B. Morgan, P. E. Pfeffer, M. Monopoli, K. A. Dawson, J. Eriksson, K. Edwards, S. Lynham, M. Arno, A. F. Behndig, A. Blomberg, G. Somers, D. Hassall, L. A. Dailey, B. Forbes and I. S. Mudway, *Nanomedicine*, 2016, **12**, 1033–1043.
50 B. Yin, C. K. W. Chan, S. Liu, H. Hong, S. H. D. Wong, L. K. C. Lee, L. W. C. Ho, L. Zhang, K. C.-F. Leung, P. C.-L. Choi, L. Bian, X. Y. Tian, M. N. Chan and C. H. J. Choi, *ACS Nano*, 2019, **13**, 14048–14069.
51 K. R. Rouillard, I. Jaspers and D. B. Hill, *Toxicol. Sci.*, 2025, **206**, 228–229.
52 D. Sanchez-Guzman, S. Boland, O. Brookes, C. Mc Cord, R. Lai Kuen, V. Sirri, A. Baeza Squiban and S. Devineau, *Sci. Rep.*, 2021, **11**, 1–14.
53 M. Dias, R. Zhang, T. Lammers and R. M. Pallares, *Drug Delivery Transl. Res.*, 2025, **15**, 789–797.
54 D. Sanchez-Guzman, P. Le Guen, B. Villeret, N. Sola, R. Le Borgne, A. Guyard, A. Kemmel, B. Crestani, J. M. Sallenave and I. Garcia-Verdugo, *Biomaterials*, 2019, **217**, 119308.
55 H. Danafar, M. N. Maleki, A. H. Moradi, A. Sharafi and K. Nedaei, *Sci. Rep.*, 2025, **15**, 14964.
56 A. Sati, T. N. Ranade, S. N. Mali, H. K. A. Yasin and A. Pratap, *ACS Omega*, 2025, **10**, 7549–7582.
57 A. A. Antsiferova, M. Y. Kopaeva, V. N. Kochkin and P. K. Kashkarov, *Nanomaterials*, 2021, **11**, 1–13.
58 H. J. Johnston, G. Hutchison, F. M. Christensen, S. Peters, S. Hankin and V. Stone, *Crit. Rev. Toxicol.*, 2010, **40**, 328–346.
59 C. Chivé, C. Mc Cord, D. Sanchez-Guzman, O. Brookes, P. Joseph, R. Lai Kuen, G. Phan, A. Baeza-Squiban, S. Devineau and S. Boland, *Environ. Toxicol. Pharmacol.*, 2023, **103**, 104281.
60 H. M. Braakhuis, I. Gosens, P. Krystek, J. A. F. Boere, F. R. Cassee, P. H. B. Fokkens, J. A. Post, H. van Loveren and M. V. D. Z. Park, *Part. Fibre Toxicol.*, 2014, **11**, 49.
61 M. Wiemann, A. Vennemann, F. Blaske, M. Sperling and U. Karst, *Nanomaterials*, 2017, **7**, 441.
62 J. N. Smith, D. G. Thomas, H. Jolley, V. K. Kodali, M. H. Littke, P. Munusamy, D. R. Baer, M. J. Gaffrey, B. D. Thrall and J. G. Teeguarden, *Part. Fibre Toxicol.*, 2018, **15**, 47.
63 N. Hadrup, A. K. Sharma, K. Loeschner and N. R. Jacobsen, *Regul. Toxicol. Pharmacol.*, 2020, **115**, 104690.
64 B. A. Weldon, E. M. Faustman, G. Oberdörster, T. Workman, W. C. Griffith, C. Kneuer and I. J. Yu, *Nanotoxicology*, 2016, **10**, 945–956.
65 T. Miclăuş, C. Beer, J. Chevallier, C. Scavenius, V. E. Bochenkov, J. J. Enghild and D. S. Sutherland, *Nat. Commun.*, 2016, **7**, 11770.
66 O. Brookes, S. Boland, R. Lai Kuen, D. Miremont, J. Movassat and A. Baeza-Squiban, *PLoS One*, 2021, **16**, 1–23.
67 D. Sanchez-Guzman, PhD thesis, Université de Paris, 2021.
68 Joint Research Centre, *Series of representative manufactured nanomaterials – NM-300 silver characterisation, stability, homogeneity*, Publications Office of the European Union, 2011.
69 J. G. Keller, M. Persson, P. Müller, L. Ma-Hock, K. Werle, J. Arts, R. Landsiedel and W. Wohlleben, *NanoImpact*, 2021, **23**, 100341.
70 M. P. Monopoli, A. S. Pitek, I. Lynch and K. A. Dawson, in *Nanomaterial Interfaces in Biology: Methods and Protocols*, ed. P. Bergese and K. Hamad-Schifferli, Humana Press, U. S.A., 2013, pp. 137–155.
71 H. Noh and E. A. Vogler, *Biomaterials*, 2007, **28**, 405–422.
72 R. Gupta, G. Radicioni, S. Abdelwahab, H. Dang, J. Carpenter, M. Chua, P. A. Mieczkowski, J. T. Sheridan, S. H. Randell and M. Kesimer, *Am. J. Respir. Cell Mol. Biol.*, 2019, **60**, 209–220.
73 R. J. Simpson, H. Kalra and S. Mathivanan, *J. Extracell. Vesicles*, 2012, **1**, 1–6.
74 G. Klein, C. Mathé, M. Biola-Clier, S. Devineau, E. Drouineau, E. Hatem, L. Marichal, B. Alonso, J. C. Gaillard, G. Lagniel, J. Armengaud, M. Carrière, S. Chédin, Y. Boulard, S. Pin, J. P. Renault, J. C. Aude and J. Labarre, *Nanotoxicology*, 2016, **10**, 1555–1564.
75 L. Böhmert, B. Niemann, D. Lichtenstein, S. Juling and A. Lampen, *Nanotoxicology*, 2015, **9**, 852–860.
76 G. H. Dar, C. C. Mendes, W.-L. Kuan, A. A. Speciale, M. Conceição, A. Görgens, I. Uliyakina, M. J. Lobo, W. F. Lim, S. El Andaloussi, I. Mäger, T. C. Roberts, R. A. Barker, D. C. I. Goberdhan, C. Wilson and M. J. A. Wood, *Nat. Commun.*, 2021, **12**, 6666.
77 J. Y. Lock, T. L. Carlson and R. L. Carrier, *Adv. Drug Delivery Rev.*, 2018, **124**, 34–49.
78 B. S. Schuster, J. S. Suk, G. F. Woodworth and J. Hanes, *Biomaterials*, 2013, **34**, 3439–3446.
79 D. B. Hill, P. A. Vasquez, J. Mellnik, S. A. McKinley, A. Vose, F. Mu, A. G. Henderson, S. H. Donaldson, N. E. Alexis, R. C. Boucher and M. G. Forest, *PLoS One*, 2014, **9**, 1–11.
80 A. Stern, A. P. Petersen, H. C. Zierden and G. A. Duncan, *Cell Biomater.*, 2025, **1**, 100043.
81 J. F. V. Rodrigues, G. A. P. de Souza, J. S. Abrahão, R. P. Amaral, R. F. G. de Castro, L. C. C. Malaquias and L. F. L. Coelho, *Biochim. Biophys. Acta*, 2022, **1866**, 130116.

82 Z. Ferdous and A. Nemmar, *Int. J. Mol. Sci.*, 2020, **21**, 2375.
83 B. Chen, P. Yu, W. N. Chan, F. Xie, Y. Zhang, L. Liang, K. T. Leung, K. W. Lo, J. Yu, G. M. K. Tse, W. Kang and K. F. To, *Signal Transduction Targeted Ther.*, 2024, **9**, 6.
84 J. M. Carnino, H. Lee and Y. Jin, *Respir. Res.*, 2019, **20**, 240.
85 F. Zhang, G. V. Aquino, A. Dabi and E. D. Bruce, *Toxicol. in Vitro*, 2019, **56**, 1–9.
86 S. Han, R. da Costa-Marques, J. Simon, A. Kaltbeitzel, K. Koynov, K. Landfester, V. Mailänder and I. Lieberwirth, *Nat. Commun.*, 2023, **14**, 295.
87 H. Lee, *Mol. Pharm.*, 2025, **22**, 2590–2602.
88 S. Subramaniam, P. Joyce and C. A. Prestidge, *Eur. J. Pharm. Biopharm.*, 2024, **202**, 114420.
89 N. V. Konduru, R. M. Molina, A. Swami, F. Damiani, G. Pyrgiotakis, P. Lin, P. Andreozzi, T. C. Donaghey, P. Demokritou, S. Krol, W. Kreyling and J. D. Brain, *Part. Fibre Toxicol.*, 2017, **14**, 1–12.
90 S. Behzadi, V. Serpooshan, W. Tao, M. A. Hamaly, M. Y. Alkawareek, E. C. Dreaden, D. Brown, A. M. Alkilany, O. C. Farokhzad and M. Mahmoudi, *Chem. Soc. Rev.*, 2017, **46**, 4218–4244.
91 M. G. Soliman, A. Martinez-Serra, M. Dobricic, D. N. Trinh, J. Cheeseman, D. I. R. Spencer and M. P. Monopoli, *Front. Toxicol.*, 2024, **6**, 1–25.
92 J. Cox, N. Neuhauser, A. Michalski, R. A. Scheltema, J. V. Olsen and M. Mann, *J. Proteome Res.*, 2011, **10**, 1794–1805.
93 S. Tyanova and J. Cox, *Methods Mol. Biol.*, 2018, **1711**, 133–148.
94 R. Kolde, *Pheatmap: Pretty Heatmaps, R package version 1.0.12*, 2019.
95 L. Kolberg, U. Raudvere, I. Kuzmin, P. Adler, J. Vilo and H. Peterson, *Nucleic Acids Res.*, 2023, **51**, 207–212.